ORIGINAL PAPER

Adsorption and spin state properties of Cr, Ni, Mo, and Pt deposited on Li$^+$ and Na$^+$ monovalent cation impurities of MgO (001) surface: DFT calculations

**Ahmad S. Shalabi · Mervat M. Assem ·
Kamal A. Soliman**

Abstract We have analyzed, by means of density functional theory calculations and the embedded cluster model, the adsorption and spin-state properties of Cr, Ni, Mo, and Pt deposited on a MgO crystal. We considered deposition at the Mg^{2+} site of a defect-free surface and at Li$^+$ and Na$^+$ sites of impurity-containing surfaces. To avoid artificial polarization effects, clusters of moderate sizes with no border anions were embedded in simulated Coulomb fields that closely approximate the Madelung fields of the host surfaces. The interaction between a transition metal atom and a surface results from a competition between Hund's rule for the adsorbed atom and the formation of a chemical bond at the interface. We found that the adsorption energies of the metal atoms are significantly enhanced by the cation impurities, and the adsorption energies of the low-spin states of spin-quenched complexes are always more favorable than those of the high-spin states. Spin polarization effects tend to preserve the spin states of the adsorbed atoms relative to those of the isolated atoms. The metal–support interactions stabilize the low-spin states of the adsorbed metals with respect to the isolated metals, but the effect is not always enough to quench the spin. Spin quenching occurs for Cr and Mo complexes at the Mg^{2+} site of the pure surface and at Li$^+$ and Na$^+$ sites of the impurity-containing surfaces. Variations of the spin-state properties of free metals and of the adsorption and spin-state properties of metal complexes are correlated with the energies of the frontier orbitals. The electrostatic potential energy curves provide further understanding of the nature of the examined properties.

A. S. Shalabi (✉) · M. M. Assem · K. A. Soliman
Department of Chemistry, Faculty of Science, Benha University,
P.O.Box 13518, Benha, Egypt
e-mail: asshalabi@hotmail.com

Introduction

Point defects and impurity atoms on metal oxide surfaces affect adsorption properties of small molecules and metal clusters and how they modulate the reactivity of adsorbed transition metal clusters; these effects are important in nanocluster catalysts, corrosion, coatings, microelectronics, and films [1–3]. Impurity atoms in MgO can be either cations replacing Mg^{2+} or anions substituting O^{2-} [4, 5]; in either case, the surface reactivity is significantly modified by their presence. In the case of cation impurities, the change depends on the charge. If Mg^{2+} is replaced by a doubly charged cation, e.g., Co^{2+} or Ni^{2+} [6], the local electronic structure changes to reflect the size of the ion, the change in covalent character of the surface–adatom interaction, and with the difference in occupancy of d orbitals. If Mg^{2+} is replaced by a singly-charged cation, e.g., Li$^+$ or Na$^+$, the electronic structure changes qualitatively, with the nearby anion formally changing its charge from −2 to −1.

Sushko et al. [7] calculated the properties of cyanide in sodium chloride crystal and demonstrated that Mott-Littleton calculations can predict the relative stability of different configurations of a family of defects. Rodriguez and Maiti [8] found that replacing some of the metal centers of MgO(001) surface with Ni atoms enhances the binding of the S-containing species through new electronic states associated with the Ni 3d levels and located above the occupied O 2p and Mg 3 s bands. They also inferred a negative correlation between the reactivity of the oxide and the size of the electronic band gap, with the chemical

activity of an oxide depending mainly on how well its bands mix with the orbitals of H₂S. Rodriguez et al. [9] examined the reaction of H_2S with MgO (001) and Cu/MgO (001) surfaces, and they reported that smaller band gaps in the oxide are associated with greater reactivity towards H_2S; they concluded that this trend reflects band–orbital mixing. Neyman and Rösch [10] performed density functional calculations for bonding and vibrations of CO molecules adsorbed at transition metal impurity sites (Co^{2+}, Ni^{2+}, Cu^{2+}) on the MgO (001) surface. The calculations qualitatively reproduced observed trends in the adsorption-induced frequency shifts for a series of surface aggregates and corresponding changes of the infrared intensities of the C–O vibrational mode. Zuo et al. [11] examined the lithium trapped-hole center in MgO and showed that while the Li^+ ion and the O^- ion move toward each other, the axial O^{2-} ion moves away from the Li^+ ion. Meng et al. [12] considered the charge-state (+1, +2, and +3) stability of Ni and Cu impurities in MgO and reported that the charge states are intrinsically unstable to disproportionation. These investigations stimulated our interest to understand how the adsorption properties of Cr, Ni, Mo, and Pt depend on the nature of the MgO surface when Mg^{2+} is replaced by Li^+ or Na^+.

The spin-state properties of transition metals on oxide supports have received special attention. The spin state of an adsorbed metal atom can be different depending on whether it interacts with a pure site or an impurity site [13–19]. To our knowledge, the dependence of the final spin states of Cr, Ni, Mo, and Pt deposited on the cation impurities Li^+ and Na^+ replacing the regular Mg^{2+} site of MgO(001) surface have neither been investigated theoretically nor experimentally.

Computational models

The present computations are based on the use of density functional theory and embedded cluster models, as applied previously to the description of nondefective, pure nonpolar oxide surfaces [20]. Here we study nondefective surfaces, except that they may contain an impurity. For the ionic solids MnO, FeO, CoO, NiO, CuO, and MgO, Illas and coworkers [21, 22] established that an embedded cluster model can be used as an alternative to periodic boundary conditions. The embedded cluster model involves a finite cluster that is modeled by assuming that the electronic structure of the rest of the host crystal (which constitutes the embedding medium) is the same as in the impurity-free bulk system. This approach can also be used where the embedded cluster contains an impurity [6, 23–26].

To represent the substrate without artificial flow of charge, nonstoichiometric clusters with no border anions have been embedded in arrays of point charges. This was done by following an embedding procedure reported previously for alkaline earth oxides [27–33]. First we constructed a finite ionic crystal of 292 point charges. The electric fields along the X and Y axes of this crystal are zero by symmetry, as in the host crystal. The ±2 charges on the outer shells were then modified, by using a fitting procedure, to make the Coulomb potential at the four central sites closely approximate the Madelung potential of the host crystal and to make the Coulomb potential vanish at the eight points with coordinates $(0,\pm R,\pm R)$ and $(\pm R,0,\pm R)$, where R is half the lattice distance. For MgO, R is 2.105 Å, and the modified charges are 0.818566 and 1.601818. The Coulomb potential was calculated to be 1.748 at the four central sites as compared with 1.746 for a simple cubic ionic crystal. All charged centers with Cartesian coordinates Z greater than zero were then eliminated to generate the (001) surface of MgO with 176 charged centers occupying the three-dimensional space with $Z \leq 0$. The clusters of Fig. 1 were then embedded within the central region of the crystal surface, and the electrons of the embedded clusters were included in the Hamiltonians of the ab initio calculations. Other crystal sites entered the Hamiltonian either as full or partial point charges.

Density functional calculations were performed by using the B3LYP hybrid density functional [34–38]. This has been used previously for the adsorption of metal atoms on MgO [6, 22, 39–42], although it is known to result in some systematic error [43]. The Stevens–Basch–Krauss compact effective potential CEP basis sets [44–46] were employed. For Li, O, Na, and Mg, the CEP double zeta basis set is called CEP-31 G, and the CEP triple zeta basis set is called CEP-121 G. For the heavier atoms considered here, there is only one CEP basis set.

The surface ions surrounding the impurity were allowed to relax to their perturbed equilibrium geometries. The pure surface exhibits very small relaxations, and therefore surface atoms are fixed at bulk lattice positions for the pure surface. The adsorption energies have been calculated as

$$E_{adsorption} = E_{complex} - E_{adsorbate} - E_{substrate}. \qquad (1)$$

With this choice, positive adsorption energies correspond to exothermic adsorption processes. The present computations were carried out by using the *Gaussian 98* computer program [47], and figures were generated by using the *GaussView* software.

Results and discussion

The spin-state properties of a metal atom deposited on a surface site may be viewed as resulting from a competition between Hund's rule for the adsorbed atom and the formation

Fig. 1 $Mg_{25}O_8$ cluster showing the metal adatom (M), and the impurity cation (I). (**a**) free cluster (**b**) embedded cluster
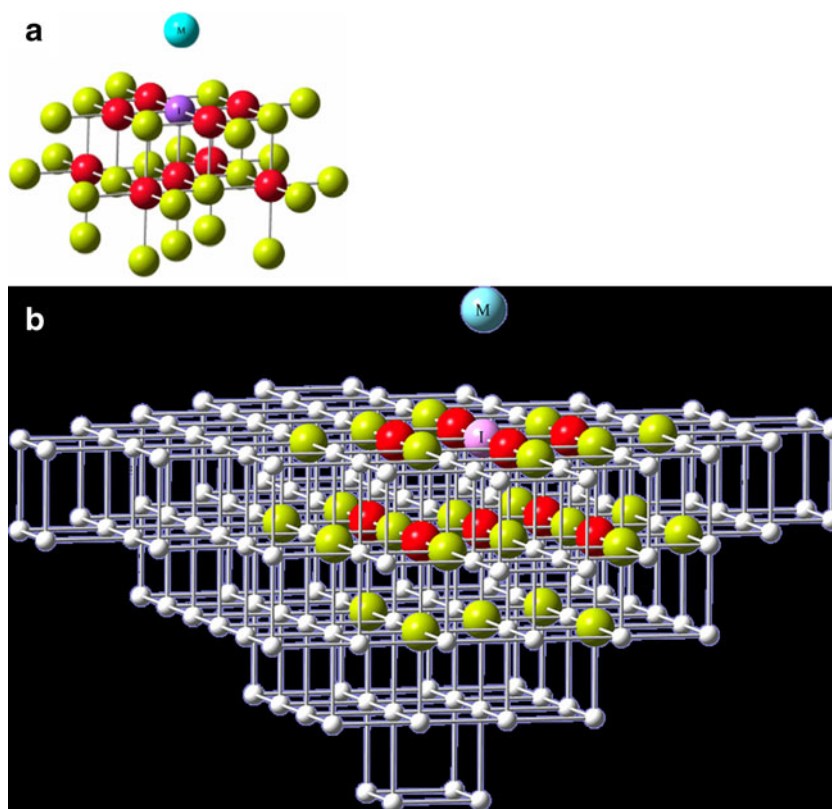
of a chemical bond at the interface [48]. The first factor favors the high-spin multiplicity within the d-manifold for a transition metal, while the second favors the low-spin multiplicity, although the quantitative strength of the favoring depends on the strength of orbital mixing [49].

In the present study, we have considered two electronic states for each case. One corresponds to low spin (L), and the other corresponds to high spin (H). In Table 1, the electronic configurations of Cr, Ni, Mo, and Pt in the gas phase are given for the high-spin and low-spin states, and the high-to-low spin transition energy is also given. The B3LYP/CEP-121 G calculation yields a high-to-low spin transition energy of 0.823 eV for Cr, which is close to the B3LYP theoretical result (0.793 eV) reported by [49] and to the experimental result (− 0.941 eV) calculated by the same

authors from the NIST atomic spectral data base. On the other hand, while our theoretical result for Ni (1.668 eV) is not in agreement with (3.000 eV) reported by Markovits et al. [49], and by Lopez et al. [48], it is closer to the experimental result (1.826 eV) reported in [49]. The reason for this discrepancy may be attributed to the different nature of the periodic calculations, and of the basis sets employed in the calculations. In [49] a plane wave basis set with a cutoff of 396 eV has been used to describe the 3d electrons of the metals and the valence electrons of MgO. The core electrons were replaced by ultrasoft pseudopotentials, and for transition metal atoms they have employed the small core relativistic pseudopotentials proposed by Hay and Wadt. They also used different Gaussian type orbitals GTO basis sets for Mg and O. The basis sets and other

Table 1 The electronic configuration , orbital diagram, spin multiplicity, spin state, and spin transition energy of Cr, Ni, Mo, and Pt

	Electronic configuration	Orbital diagram	Spin multiplicity	Spin state	$E_{atom}^{H-L}(e.V)$
^{24}Cr [Ar] $3d^54s^1$	$3d^54s^1$	↑ ↑ ↑ ↑ ↑ ↑	7	H	-0.823
	$3d^6$	↑↓ ↑ ↑ ↑ ↑	5	L	
^{28}Ni [Ar] $3d^84s^2$	$3d^84s^2$	↑↓ ↑↓ ↑↓ ↑ ↑ ↑↓	3	H	-1.668
	$3d^{10}$	↑↓ ↑↓ ↑↓ ↑↓ ↑↓	1	L	
^{42}Mo [Kr] $4d^55s^1$	$4d^55s^1$	↑ ↑ ↑ ↑ ↑ ↑	7	H	-1.008
	$3d^6$	↑↓ ↑ ↑ ↑ ↑	5	L	
^{78}Pt [xe]$4f^{14}5d^96s^1$	$5d^96s^1$	↑↓ ↑↓ ↑↓ ↑ ↑ ↑↓	3	H	-0.38 2
	$3d^{10}$	↑↓ ↑↓ ↑↓ ↑↓ ↑↓	1	L	

approaches reported in [50] are almost the same as those reported in [49].

Consider the adsorption properties and the possible spin quenching of high spin states of free metal atoms when adsorbed on the Mg^{2+} site of the defect free surface, and Li^+ and Na^+ sites of the defect containing surfaces. The nondefective MgO (001) surface exhibits very small relaxation only and therefore it has been kept fixed when examining the adsorption of metal atoms. Surface relaxation effects can be significant if discontinuities, like steps or point defects, are present [51, 52]. Table 2 summarizes the results obtained for several structure and energetic properties of Ni, Pt, Cr, and Mo deposited on the Mg^{2+} site of the defect free surface. As shown, the calculated adsorption energies in eV for the high spin states are : -2.161(Ni), -1.657(Pt), -2.528 (Cr), -2.445(Mo), and for the low spin states : -2.068(Ni), -1.302(Pt), -3.361(Cr), -3.472(Mo). Except for Pt, the adsorption energies of the four transition metals in the low spin states are significantly larger than those in the high spin states. The metal-support interactions stabilize the spin states of the adsorbed metals, with respect to those of the isolated metals, and the effects were strong enough to quench the spins, i.e, to change the sign of high to low spin transition energies from negative to positive. As shown in Table 1, the high to low spin transition energies are negative indicating that the high spin states are favored. However, upon interaction with the Mg^{2+} site of the defect free surface, Table 2, the high to low spin transition energies of Cr and Mo turn out to be positive, indicating that spin states are no longer preserved and the low spin states are energetically favored. While the adsorption energies of Cr and Mo (group VIA) in the high spin states are smaller than those in the low spin states, the adsorption energies of Ni and Pt (group VIIIA) in the high spin states are greater than those in the low spin states. Adsorption energies correlate inversely with the adsorbate-substrate distances. As the strength of adsorbate-substrate interaction increases, the corresponding adsorbate-substrate distance decreases.

Table 3 summarizes the results obtained for structure and energetic properties of Ni, Cr, Mo, and Pt deposited on the cation impurity sites, Li^+ and Na^+, of the defect containing surface. Upon metal deposition, the two impurity cations, Li^+ and Na^+, relax vertically downward. It can be seen that the magnitude of downward displacements of Li^+ is significantly larger than that of Na^+ as a logical consequence of the smaller size of Li^+ relative to Na^+. Moreover, while the nearest neighbor surface O anions surrounding the impurity cation Li^+ do not relax outward toward the nearest neighbor cations, the nearest neighbor surface O anions surrounding the impurity cation Na^+ relax outward, again as a logical consequence of the larger size of Na^+ relative to Li^+. Except for Pt, all adsorption energies in the low spin states are significantly larger than those in the high spin states, and the adsorbate-substrate equilibrium distances are linearly correlated. All adsorption energies in the high and low spin states of metals on Li^+ impurity site are significantly larger than those on the Mg^{2+} site. However, on the Na^+ site and apart from Pt, while adsorption energies in the high spin states were larger smaller than those on the Mg^{2+} site, adsorption energies in low spin states were greater than those on the Mg^{2+} counterpart. Moreover, all metal atoms get closer to the Li^+ and Na^+ sites than do to the Mg^{2+} site. This goes in line with the strength of interaction, since adsorption energies in the low spin states are greater than those in the high spin states, and may be generally explained on basis of the smaller Pauli repulsion of the defect containing surface even though there was no structure reorganization. In general terms, the behavior of a single metal atom adsorbed on a particular surface is a result of a competition between Hund's rule for the adsorbed atom and the formation of a chemical bond at the interface, where the first mechanism favors the highest multiplicity within the near degenerate d-manifold, while the second favors the largest possible coupling between electrons.

It may be interesting to compare the high-to low-spin transition energies of the free metals with the corresponding high-to low-spin transition energies of the adsorbed metals. This provides information on the change in the transition energy induced by the surface. The data given in Tables 1, 2, 3 show that in all cases, except (Pt) on the defect free surface, the energy required to go from the high to low-spin state changes significantly when the support is present. The results indicate that the spins of Ni and Pt are preserved when the support is present regardless of the adsorption site. This implies that even if the metal-support interaction tends to stabilize the low spin-state with respect to the isolated atom, this effect is not always enough to quench the spin on the defective surface.

A revisit to Table 2 shows that while the adsorption energies of Cr and Mo in the low spin states are greater

Table 2 Structural and energetic properties of Ni, Cr, Mo, and Pt deposited on the Mg^{2+} site of the defect free surface of MgO

	$E_{ads.}^{H}(e.V)$	$E_{ads.}^{L}(e.V)$	$E_{complex}^{H-L}(e.V)$	$\mathbf{r}_e^H$ A	$\mathbf{r}_e^L$ (A)
Ni	-2.161	-2.068	-1.761	2.44	2.41
Cr	-2.528	-3.361	0.010	2.78	2.75
Mo	-2.445	-3.472	0.020	2.81	2.81
Pt	-1.657	-1.302	-0.738	2.56	2.53

$E_{ads.}$: adsorption energy

$E_{complex}^{H-L}(e.V)$: spin transition energy

H:high spin

L: low spin

r: adsorbate substrate distance

Table 3 Structural and energetic properties of Ni, Cr, Mo, and Pt deposited on Li+and Na+sites of the defect containing surface of MgO

Impurity cation	Adsorbed metal	$E_{ads.}^{H}(eV)$	$E_{ads.}^{L}(eV)$	$E_{complex}^{H-L}(eV)$	$r_{M}^{H}(A)$	$r_{M}^{L}(A)$	r_{I}^{H}	r_{I}^{L}	Δr_{O}^{H}	Δr_{O}^{L}
Li^{+}	Ni	-4.273	-5.131	-0.810	1.83	1.74	-0.59	-0.61	0.01	0.00
	Cr	-4.890	-6.361	0.648	1.83	1.83	-0.62	-0.63	0.00	0.00
	Mo	-4.956	-6.617	0.653	1.96	1.96	-0.63	-0.63	0.00	0.00
	Pt	-3.461	-3.707	-0.136	2.05	1.92	-0.54	-0.59	0.03	0.00
Na^{+}	Ni	-1.975	-2.262	-1.381	2.17	2.22	-0.18	-0.23	0.08	0.08
	Cr	-2.380	-3.491	0.288	2.38	2.27	-0.14	-0.24	0.08	0.10
	Mo	-2.174	-3.675	0.493	2.36	2.27	-0.08	-0.26	0.08	0.08
	Pt	-1.483	-1.043	-0.821	2.44	2.50	-0.20	-0.07	0.09	0.05

$E_{ads.}$: adsorption energy

$E_{complex}^{H-L}$: spin transition energy

H:high spin

L: low spin

r_{M}: metal- substrate distance

r_{I}: vertical displacement of the impurity cation, where a negative value a downward displacement

Δr_{O}: horizontal displacement of surface oxygen ions surrounding the impurity cation, where a positive value denotes displacement outward

than those in the high spin states, the adsorption energies of Ni and Pt in the high spin states are greater than those in the low spin states. This may be explained on basis of the extra stability of Cr and Mo complexes in the low spin states, and Ni and Pt complexes in the high spin states. The extra stability allows for stronger interactions with the defect free surface. When we come to consider the Li^{+} and Na^{+} sites of the defect containing surfaces, the same reasoning may be applied. In Table 3, apart from deposition of Pt on Na^{+}, the adsorption energies of Ni, Cr, Mo and Pt in the low spin
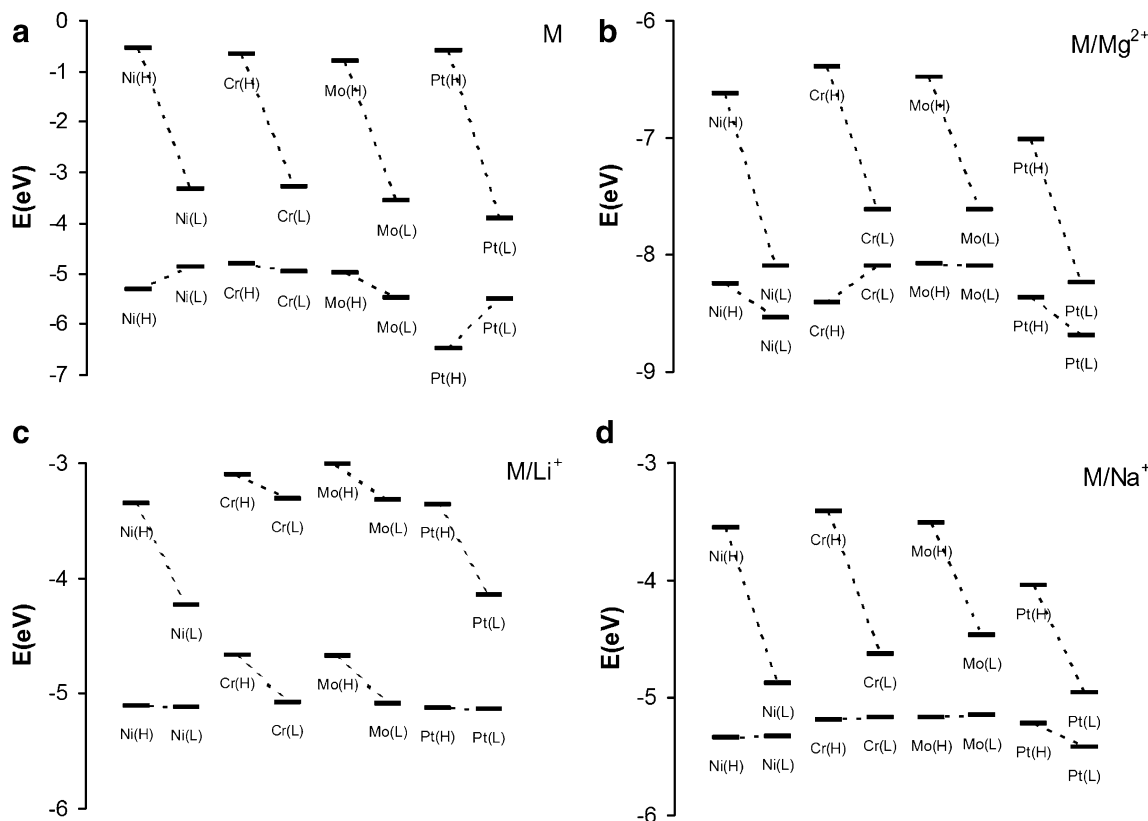
Fig. 2 Frontier orbitals of free metals and metal complexes in the high and low spin states. (**a**) free metals, (**b**) metal complexes with Mg^{2+} site, (**c**) metal complexes with Li^{+} site, and (**d**) metal complexes with Na^{+} site

Table 4 Atomic spin polarization data of Ni, Cr, Mo, and Pt deposited on Mg2+ site of the defect free surface, and Li+and Na+sites of the defect containing surfaces of MgO, high to low spin transition energy, and metal Mulliken charges

Metal	E_{UDFT}^H (E_h)	E_{RODFT}^H (E_h)	$\Delta E_{S.P}^H(DFT)$eV	site	$E_{Complex}^{H-L}$(eV)	q^H	q^L
Ni	-169.44960	-169.44814	-0.040	Mg^{2+}	-1.761	0.52	0.52
				Li^+	-0.810	-0.24	-0.32
				Na^+	1.381	0.28	0.28
Cr	-86.51021	-86.27303	-6.454	Mg^{2+}	0.010	0.96	0.93
				Li^+	0.648	-0.58	-0.62
				Na^+	0.288	0.32	0.18
Mo	-67.88161	-67.88140	-0.006	Mg^{2+}	0.020	0.80	0.79
				Li^+	0.653	-0.95	-1.00
				Na^+	0.493	0.17	0.12
Pt	-119.70322	-119.68160	-0.588	Mg^{2+}	-0.738	0.25	0.20
				Li^+	-0.136	0.09	-0.12
				Na^+	0.821	0.15	0.12

U : unrestricted

RO : restricted open

sp: spin polarization

$E_{Complex}^{H-L}$: high to low spin transition energy

q: metal Mulliken charge

states are greater than those in the high spin states. Again, this may be explained on basis of the extra stability of metal complexes in the low spin states where the metal-support interactions stabilize the low spin states of Ni and Pt and the effect is not enough to quench the spins.

Following the language of frontier orbital analysis one can see from Fig. 2 that the energy gaps between the HOMOs of the high spin states and the LUMOs of the low spin states of Cr and Mo complexes are always greater than those of Ni and Pt. Since spin quenching occurs for Cr and Mo complexes only, we can conclude that there is an inverse correlation between the process of spin quenching and the magnitude of the energy gap between the HOMO of the high spin state and the LUMO of the low spin state.

The density functional theory data using atomic symmetry for space and spin, restricted open-shell DFT (RODFT), or allowing a spin and space broken symmetry solution, unrestricted DFT (UDFT) are given in Table 4. The difference between UDFT and RODFT atomic energies is taken as a measure for spin polarization effects [49]. Spin polarization is the degree to which the spin, i.e., the intrinsic angular momentum of elementary particles, is aligned with a given direction. It may refer to (static) spin waves, preferential correlation of spin orientation with ordered lattices (semiconductors or insulators). If the UDFT and RODFT atomic energies are very close, this will indicate that spin polarization effects are rather small. The high to low spin transition energies of the metals adsorbed on Mg^{2+} site of the defect free surface and Li^+ and Na^+ sites

Table 5 Spin contamination, structural and energetic properties, and population analysis of metal complexes at the Mg^{2+} site of the defect free surface ($Mg_{26}O_9$)

Complex	2 S+1	‹s^2›	s (s +1)	Spin contamination	r_e (Å)	Mulliken spin density	Mulliken charge	Natural charge	Natural population (total)
Ni	1	0.0	0.0	0.0	2.41		0.52	0.66	27.34
	3	2.006	2	0.006	2.44	0.92	0.52	-0.15	14.15
Cr	5	7.019	6	1.019	2.75	5.25	0.93	-2.13	14.13
	7	12.015	12	0.015	2.78	4.99	0.96	0.78	23.22
Mo	5	7.020	6	1.020	2.81	5.16	0.79	0.75	41.25
	7	12.019	12	0.019	2.81	5.03	0.80	-2.07	23.07
Pt	1	0.0	0.0	0.0	2.53		0.19	0.29	77.71
	3	2.044	2	0.044	2.56	0.83	0.25	-0.28	39.28

(2 S+1): spin multiplicity

S: $\sum_i s_i$ total spin or 1/2 the number of unpaired electrons

‹s^2›: average value of total spin

[‹s^2› - S(S+1)]: spin contamination

r_e: adsorbate-substrate distance

H : High spin

L : Low spin

Table 6 Spin contamination, structural and energetic properties, and population analysis of metal complexes at the Li$^+$ site of the cation impurity surface (Mg$_{26}$O$_9$)

Complex	2 S+1	$\langle s^2 \rangle$	s (s +1)	Spin contamination	r_e (Å)	Mulliken spin density	Mulliken charge	Natural charge	Natural population (total)
Ni	1	0.0	0.0	0.0	1.74		-0.32	0.93	27.07
	3	2.0109	2	0.0109	1.83	1.39	-0.24	1.11	26.89
Cr	5	6.0629	6	0.0629	1.83	4.09	-0.62	1.22	22.78
	7	12.064	12	0.064	1.83	4.20	-0.58	1.23	22.77
Mo	5	6.0272	6	0.0272	1.96	3.88	-1.00	1.14	40.86
	7	12.027	12	0.027	1.96	4.02	-0.95	1.16	40.84
Pt	1	0.0	0.0	0.0	1.92		-0.12	0.76	77.24
	3	2.023	2	0.0229	2.05	0.97	0.09	0.73	77.27

(2 S+1): spin multiplicity

S: $\sum_i s_i$ total spin or ½ the number of unpaired electrons

$\langle s^2 \rangle$: average value of total spin

[$\langle s^2 \rangle$ - S(S+1)]: spin contamination

r_e: adsorbate-substrate distance

H : High spin

L : Low spin

of the defect containing surface are given in Table 4 for correlation with the atomic spin polarization data. As can be seen, for the same group of transition metals , Ni and Pt in group (VIII) and Cr and Mo of group (VIA), spin polarization effects are inversely correlated with spin transition energies, i.e, the larger the former the smaller the latter. This in turn implies that spin polarization effects tends to reverse the spin states of adsorbed metals with respect to those of the free metals. Hence spin polarization tends to quench the spins of the transition metals within the same group regardless of the adsorption site, Mg^{2+} of the defect free surface or Li$^+$ and Na$^+$ sites of the defect containing surface at the DFT level of theory.

The positive charge distribution on the metals that are deposited on the surface cations of MgO, Table 4, suggests that while charge transfer takes place from the metals to the Mg^{2+} and Na$^+$ surface sites, it takes place from the Li$^+$ surface sites to the metals. This may be explained on basis

Table 7 Spin contamination, structural and energetic properties, and population analysis of metal complexes at the Na$^+$ site of the cation impurity surface(Mg$_{26}$O$_9$)

Complex	2 S+1	$\langle s^2 \rangle$	s (s +1)	Spin contamination	r_e (Å)	Mulliken spin density	Mulliken charge	Natural charge	Natural population (total)
Ni	1	0.0	0.0	0.0	2.22		0.28	0.79	27.21
	3	2.0443	2	0.0443	2.17	0.97	0.28	0.71	27.29
Cr	5	6.7193	6	0.7193	2.27	5.00	0.18	0.94	23.06
	7	12.0167	12	0.0167	2.38	5.02	0.32	0.80	23.20
Mo	5	6.4767	6	0.4767	2.27	4.77	0.12	0.98	41.02
	7	12.0140	12	0.014	2.36	5.21	0.17	0.78	41.22
Pt	1	0.0	0.0	0.0	2.50		0.12	0.45	77.54
	3	2.0955	2	0.0955	2.44	0.54	0.15	0.40	77.60

(2 S+1): spin multiplicity

S: $\sum_i s_i$ total spin or ½ the number of unpaired electrons

$\langle s^2 \rangle$: average value of total spin

[$\langle s^2 \rangle$ - S(S+1)]: spin contamination

r_e: adsorbate-substrate distance

H : High spin

L : Low spin
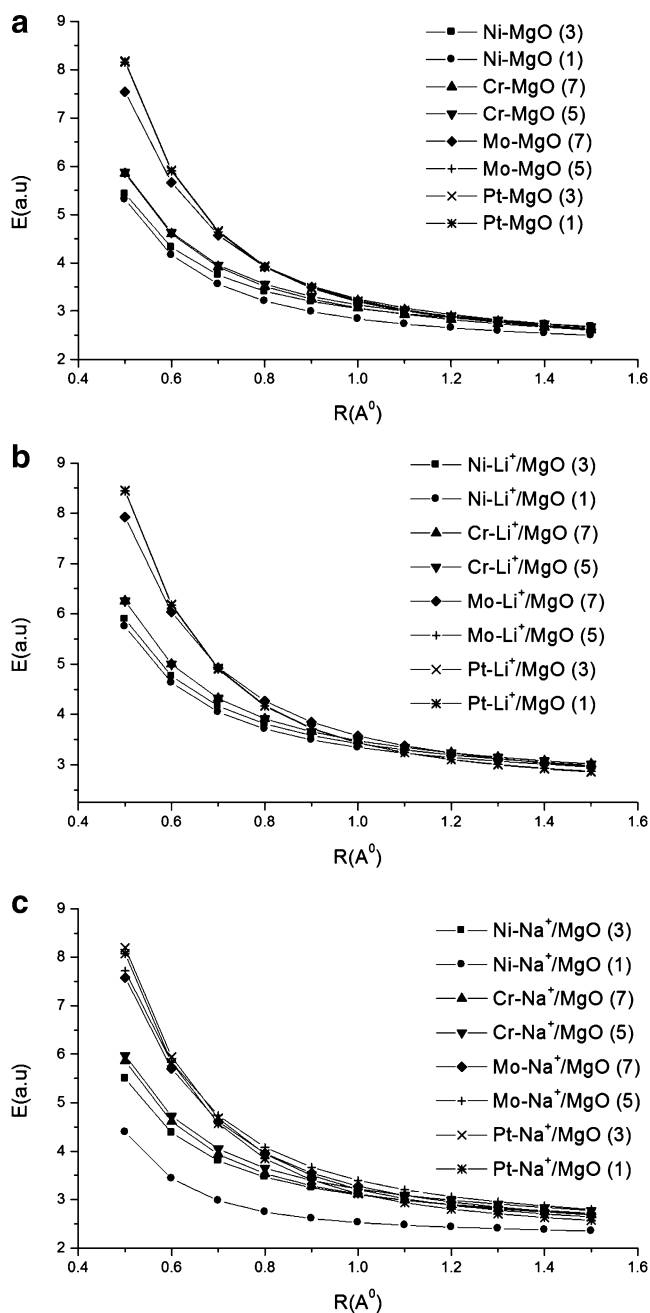
Fig. 3 Collective electrostatic potential energy curves E(a.u) as functions of the distances perpendicular to the surface site R(A°) for metal complexes in the high spin states. (**a**) Mg2+ site (**b**) Li+ site (**c**) Na+ site

of the larger effective nuclear charges of Mg^{2+} and Na^+ cations compared with that of Li^+ cation.

For systems with a spin multiplicity other than one, it is not possible to use the restricted Hartree-Fock or density functional theory method as is. In an unrestricted calculation, there are two complete sets of orbitals, one for the alpha electrons and one for the beta electrons. Usually these two sets of orbitals use the same set of basis functions but different molecular orbital coefficients. The advantage of

UHF or UDFT calculations is that they can be performed very efficiently. The disadvantage is that the wave function is no longer an Eigenfunction of the total spin, $<S^2>$, thus some error may be introduced into the calculation. This error is called spin contamination. Spin contamination results in having wave functions which appear to be the desired spin state, but have a bit of some other spin state mixed in. This occasionally results in slightly lowering the computed total energy due to having more variational freedom. Since this is not a systematic error, the difference in energy between states will be adversely affected. A high spin contamination can affect the geometry and population analysis and significantly affect the spin density.

As a check for the presence of spin contamination, we report the expectation value of the total spin, $<S^2>$, Tables 5, 6, 7. If there is no spin contamination this should equal S(S+ 1) where S equals half times the number of unpaired electrons. To examine how spin contamination affects the results, we report the adsorbate substrate distance r_e, Mulliken spin density, Mulliken charge, natural charge, and natural total population obtained from the method of natural bond orbital analysis NBO, in addition to the spin transition energy $E_{complex}^{H-L}$ of Ni, Cr, Mo, and Pt low and high spin complexes at the defect free and defect containing surfaces. Despite that it is less common to find significant spin contamination in DFT calculations, Tables 5, 6, 7 show that spin contaminations of Cr and Mo low spin complexes at the defect free surface of MgO can be significant. In Table 5, spin contamination of the low spin complexes of Cr and Mo are significantly greater than those of Ni and Pt. This is correlated linearly with the adsorbate-substrate distance, Mulliken spin density, Mulliken charge, and natural charge, and inversely with the total natural population, spin transition energies, and adsorption energies, see Table 2 for the last quantity. Most of the previous trends observed for metal complexes on the Mg^{2+} site of the defect free surface are also observed for Li^+ and Na^+ sites of the defect containing surfaces, Tables 6 and 7.

We aim now to establish relations between atomic or molecular frontier orbitals at one hand, and the adsorption and spin state properties at the other hand. The highest occupied atomic orbitals HOAOs and lowest unoccupied atomic orbitals LUAOs of the free metals, and the highest occupied molecular orbitals HOMOs and lowest unoccupied molecular orbitals LUMOs of metal complexes at the Mg^{2+} site of the defect free surface, and Li^+ and Na^+ sites of the defect containing surfaces of MgO are collected in Fig. 2. As can be seen, the LUAOs of the free metals either in their high or low spin states are comparable in energies in consistence with their spin preservation property, namely, the high spin states are always energetically preferred than that of the low spin states. When we come to consider metals in complexes, the LUMOs of complexes in their

high and low spin states exhibit linear correlations with adsorption energies, Tables 2 and 3. The LUMOs of Cr and Mo complexes are always greater than those of Ni and Pt. The adsorption energies of Cr and Mo complexes in their high and low spin states are also greater than those of Ni and Pt counterparts. On the other hand, spin quenching occurs for Cr and Mo complexes that are characterized with high LUMOs relative to those of Ni and Pt counterparts. Moreover, as evident from Tables 2 and 3, the low spin complexes of Cr and Mo are more stable than their high spin counterparts in contrast with Ni and Pt complexes. This extra stability allows for stronger interaction with the surface. In other words, the interaction in this case is strong enough to quench the spin, and spin pairing mechanism dominates Hund's rule.

Finally, in order to understand the possible electrostatic contributions to the defect free and defect containing surfaces, and to provide further rationalization and characterization of adsorption and spin quenching properties, we calculated the electrostatic potentials over the Mg^{2+} site of the defect free surface, and Li^+ and Na^+ sites of the defect containing surface, Fig. 3. The electrostatic potential curves E(a.u) are given as functions of the distances perpendicular to the surface $R(A^0)$. As shown, the electrostatic potentials provide unique characterization of surface sites. The electrostatic potential curves of the spin quenched complexes of Cr and Mo are symmetrically distributed between those of Ni and Pt complexes, increase as the perpendicular distances to the surface decrease, and converge at approximately 1.5 A^0 above the surface. The high and low spin electrostatic contributions of each complex split at approximately 0.5 A^0 above the surface. No negative electrostatic potentials were detected and the strength of electrostatic contributions of metal complexes follows the order Pt>Mo> Cr>Ni. The electrostatic potential contributions to the low spin states of metal complexes are greater than those of the high spin states at about 0.5 A^o from the surface and coincide at larger distances. Adsorption and spin quenched properties of complexes at the defect free and defect containing surfaces are therefore characterized, and the observed behavior is basically attributed to the metal surface interactions. More specifically, the interaction between the d_{z^2} electrons of the metal, and the outer valence electrons of Mg^{2+}, Li^+ and Na^+ cations.

Conclusions

An attempt has been made to understand the simultaneous adsorption –spin state behavior of a set of transition metals deposited on Mg^{2+} site of the defect free surface, and the Li^+ and Na^+ impurity sites of the defect containing surfaces of MgO. This behavior results from a competition between

chemical bonding and magnetism, and is important to understand the role of the support and the considerable practical and technological consequences. In this case, it should be possible prepare oxide surfaces where adsorbed metal atoms exhibit selected nonmagnetic or magnetic ground state. For example, the reactivity of adsorbed metal atoms will be different depending on whether the magnetic moment is quenched or not.

From the set of results presented in this work it appears that the strength of adsorbate-substrate interactions, and the possible quenching of magnetic moment of adsorbed metals on an oxide surface are strongly dependent on the choice of the metal and the support. Spin polarization and contamination as well as electrostatic potentials can characterize the adsorption and spin state properties at the defect free and defect containing (001) surfaces of MgO. Theoretical calculations should explicitly consider the open shell character of the adsorbate.

References

1. Henrich VE, Cox PA (1994) The Surface Science of Metal Oxides. Cambridge University Press, Cambridge
2. Noguera C (1996) Physics and Chemistry at Oxide Surfaces. Cambridge University Press, Cambridge
3. Freund HJ (2002) Surf Sci 500:271–299
4. Pacchioni G (2001) Oxide Surfaces. In: Woodruff DP (ed) The Chemical Physics of Solid Surfaces, Vol 9. Elsevier, Amsterdam
5. Pacchioni G (2000) Surf Rev Lett 7:277–306
6. Valero R, Gomes JRB, Truhlar DG, Illas F (2010) J Chem Phys 132:104701(1–13)
7. Sushko PV, Shluger AL, Baetzold RC, Catlow CRA (2000) J Phys Condens Matter 12:8257–8266
8. Rodriguez JA, Maiti A (2000) J Phys Chem B 104:3630–3638
9. Rodriguez JA, Jirsak T, Chaturvedi S (1999) J Chem Phys 111:8077–8087
10. Neyman KM, Rösch N (1993) Chem Phys 177:561–570
11. Zuo J, Panedy R, Kunz AB (1991) Phys Rev B 44:7187–7191
12. Meng J, Vail JM, Stoenham AM, Jena P (1990) Phys Rev B 42:1156–1162
13. Yudanov I, Pacchioni G, Neyman K, Rösch N (1997) J Phys Chem B 101:2786–2792
14. Giordano L, Pacchioni G, Ferrari AM, Illas F, Rösch N (2001) Surf Sci 432:213–226
15. Giordano L, Pacchioni G, Illas F, Rösch N (2001) Surf Sci 499:73–84
16. Lopez N, Paniagua JC, Illas F (2002) J Chem Phys 117:9445–9451
17. Markovits A, Paniagua JC, Lopez N, Minot C, Illas F (2003) Phys Rev B 67:115417(1–6)
18. Abdel Halim WS, Shalabi AS, Ghonaim MS (2009) Int J Quantum Chem 109:1094–1102
19. Shalabi AS, Abdel Halim WS, Ghonaim MS (2010) Phys B 406:397–405
20. Jaffe E, Pandey R, Kunz AB (1991) Phys Rev B 43:14030–14034
21. Sousa C, de Graaf C, Lopez N, Harrison NM, Illas F (2004) J Phys Condens Matter 16:S2557–S2574
22. Valero R, Gomes JRB, Truhlar DG, Illas F (2008) J Chem Phys 129:124710(1–7)

23. Scorza E, Birkenheuer U, Pisani C (1997) J Chem Phys 107:9645–9658
24. D'Ercole A, Giamello E, Pisani C, Ojamae L (1999) J Phys Chem 103:3872–3876
25. Ojamae L, Pisani C (1998) J Chem Phys 109:10984–10995
26. D'Ercole A, Pisani C (1999) J Chem Phys 111:9743–9753
27. Shalabi AS, El-Mahdy AM (2001) Phys Lett A 281:176–186
28. Shalabi AS (2002) J Mol Model 8:1104–1120
29. Abdel Halim WS, Shalabi AS (2002) Solid State Commun 124:67–72
30. Abdel Halim WS, Shalabi AS (2004) Appl Surf Sci 221:53–61
31. Shalabi AS, Kamel MA, Ammar HY (2005) Int J Quantum Chem 103:432–448
32. Shalabi AS, Abdel Aal S, Kamel MA, Taha HO, Ammar HY, Abdel Halim WS (2006) Chem Phys 328:8–16
33. Abdel Halim WS, Assem MM, Shalabi AS, Soliman KA (2009) Appl Surf Sci 255:7547–7555
34. Becke AD (1988) Phys Rev A 38:3098–3100
35. Becke AD (1993) J Chem Phys 98:5648–5652
36. Stephens PJ, Devlin FJ, Chabalowski CF, Frisch MJ (1994) J Phys Chem 98:11623–11627
37. Vosko SH, Wilk L, Nusair M (1980) Can J Phys 58:1200–1211
38. Lee C, Yang W, Parr RG (1988) Phys Rev B 37:785–789
39. Lopez N, Illas F, Rösch N, Pacchioni G (1999) J Chem Phys 110:4873–4879
40. Martyin RL, Illas F (1997) Phys Rev Lett 79:1539–1542
41. Moreira IPR, Illas F, Martin RL (2002) Phys Rev B 65:1551021–15510214
42. Lopez N, Illas F (1998) J Chem Phys B 102:1430–1436
43. Caballol R, Castell O, Illas F, Malrieu JP, Moreira IPR (1997) J Phys Chem A 101:7860–7866
44. Stevens W, Basch H, Krauss J (1984) J Chem Phys 81:6026–6033
45. Stevens W, Krauss M, Basch H, Jasien PG (1992) Can J Chem 70:612–630
46. Cundari TR, Stevens WJ (1993) J Chem Phys 98:5555–5565
47. Frisch MJ et al (1998) Gaussian 98. Gaussian Inc, Pittsburgh, PA
48. Markovits A, Skalli MK, Minot C, Pacchioni G, Lopez N, Illas F (2001) J Chem Phys 115:8172–8177
49. Salem L, Leforestier C (1979) Surf Sci 82:390–412
50. Mori Sanchez P, Recio JM, Silvi B, Sousa C, Martin Pendas A, Luana V, Illas F (2002) Phys Rev B 66:075103(1–6)
51. Neyman KM, Inntam C, Nasluzov VA, Kosarev R, Rösch N (2004) Appl Phys A 78:823–828
52. Florez E, Mondragon F, Fuentealba P, Illas F (2008) Phys Rev B 78:075426(1–7)